Hindawi
Geofluids
Volume 2021, Article ID 6698649, 13 pages
https://doi.org/10.1155/2021/6698649

Research Article

Experimental Study on the Propagation Characteristics of Hydraulic Fracture in Clayey-Silt Sediments

Cheng Lu,[1,2,3,4,5] **Xuwen Qin**,[1,2,3,6] **Wenjing Mao**,[1,2,3] **Chao Ma**,[1,2,3] **Lantao Geng**,[1,2,3] **Lu Yu**,[1,2,3] **Hang Bian**,[3,5] **Fanle Meng**,[1,2,3] **and Rongrong Qi**[1,2,3]

[1]*Guangzhou Marine Geological Survey, China Geological Survey, Guangzhou 510760, China*
[2]*Gas Hydrate Engineering Technology Center, China Geological Survey, Guangzhou 510760, China*
[3]*Southern Marine Science and Engineering Guangdong Laboratory (Guangzhou), Guangzhou 511458, China*
[4]*Center of Oil & Natural Gas Resource Exploration, China Geological Survey, Beijing 100083, China*
[5]*School of Energy Resources, China University of Geosciences, Beijing 100083, China*
[6]*China Geological Survey, Beijing 100083, China*

Correspondence should be addressed to Cheng Lu; jaluch@126.com and Wenjing Mao; inoswissfin826@163.com

Received 31 December 2020; Revised 6 April 2021; Accepted 29 July 2021; Published 14 August 2021

Academic Editor: Guo Chaobin

The low permeability of clayey-silt hydrate reservoirs in the South China Sea affects the thermal and pressure conductivity of the reservoir, which is difficult to spread to the far end of the wellbore and achieve commercial gas production. In this respect, enhancing the permeability to assist depressurization is necessary. Hydraulic fracturing is a promising reservoir stimulation method for gas hydrate reservoirs. Up to now, majorities of research focus on the fracability of hydrate-bearing sandy sediments, but the studies rarely involved fracture propagation characteristics of clayey-silt sediments in the hydrate dissociation area. In this paper, three sets of hydraulic fracturing experiments under different confining pressure were carried out using the clayey-silt sediments in the Shenhu Area. Computed tomographic (CT) images indicated that clayey-silt sediments could be artificially fractured, and the fracturing fluid could induce tensile fractures and local shear fractures. A multimorphological fracture zone occurred near the borehole. Furthermore, the greater the confining pressure imposed, the greater the breakdown pressure was, and the microfracture arose more easily. The fractures at the top were generally wider than those at the bottom with the same confining pressure. The experimental results could reveal the fracture initiation and propagation mechanism of clayey-silt sediments and provide theoretical support for hydraulic fracture in the hydrate dissociation area.

1. Introduction

Natural gas hydrates are crystalline material formed by natural gas and water at high pressure and low temperature. Its global resource is estimated that more than twice the total amount of proven traditional fossil energy resources [1–4]. However, 90% of the gas hydrates in nature exist in marine clayey-silt or silt sediments [5–7], with characteristics of low formation temperature, weak cementation, nondiagenesis, and low permeability [8–13]. There could be a potential risk for methane leak, sand production, stratum settlement, and so on in long-term exploitation, which greatly limits the hydrate productivity [5, 14, 15]. So far, the natural gas hydrate reservoir production tests imply that the gas production via depressurization is still far from reaching the commercial level [16–19].

Yu et al. [20] adopted the special production strategies of aggressive depressurization and permeability improvement and conducted long-term numerical simulations to contrast the gas recovery enhancement with different production strategies. They concluded that the permeability improvement, which raised the average gas production rate by one order of magnitude, might be more reliable than the aggressive depressurization on the gas recovery enhancement. Hence, enhancing the permeability to assist depressurization is necessary [21–25].

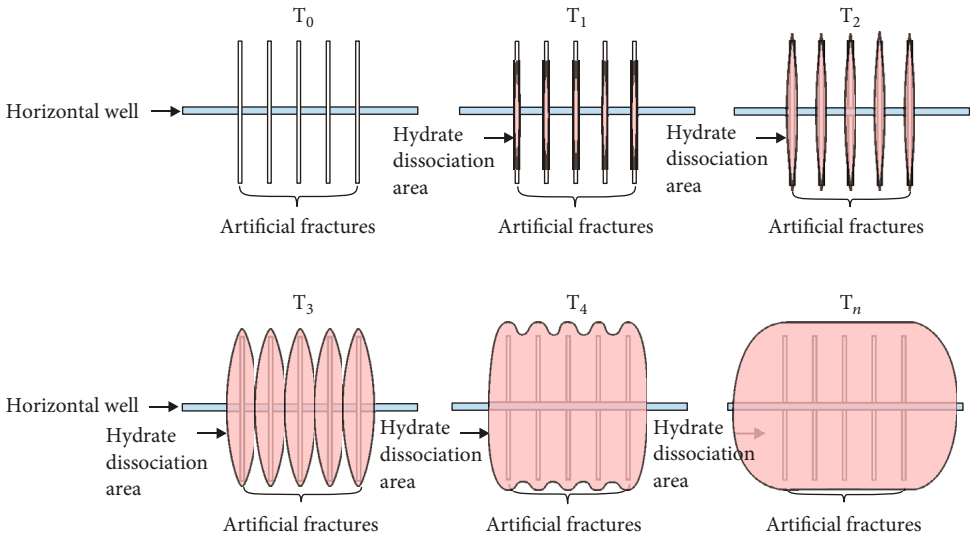

Figure 1: Illustration of hydraulic fracture in the hydrate dissociation area for a horizontal well.

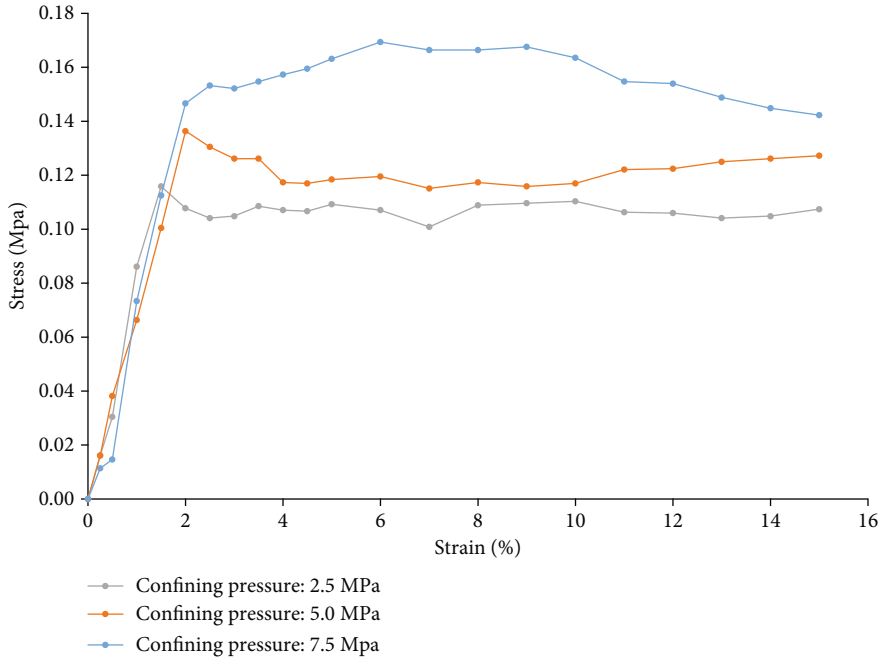

Figure 2: Stress-strain relationship of clayey-silt sediments [38].

Hydraulic fracturing is an effective stimulation method for increasing the permeability in unconventional resources. It could create artificial fractures in gas hydrate layers, strengthen the seepage capacity between wellbore and dissociation boundary, accelerate pressure propagation, improve thermal transfer efficiency [14, 26, 27], and enlarge the hydrate dissociation area so as to promote gas and water to rapidly flow to the wellbore through fractures and enhance well production of low-permeability reservoirs (Figure 1).

To understand the fracture propagation characteristics of hydrate-bearing sediments, laboratory and numerical studies have been conducted [28–32]. Konno et al. [28] combined hydraulic fracturing triaxial experiment and X-CT scanning to investigate fracture behavior. They found that the permeability of unconsolidated sandy sediments could be improved significantly due to crystal-crystal and crystal-sand boundaries activated by hydraulic fracturing. Too et al. [29] utilized a thin circular plastic sheet to form natural fracture and indicated that laboratory synthesized hydrate-bearing sandy sediments with the saturation of 50-75% could create new fractures and propagate the natural fractures. Liu et al. [30] built a novel feasibility evaluation model of hydraulic fracturing in hydrate-bearing sediments and indicated that higher fracturing fluid displacement would produce greater flow

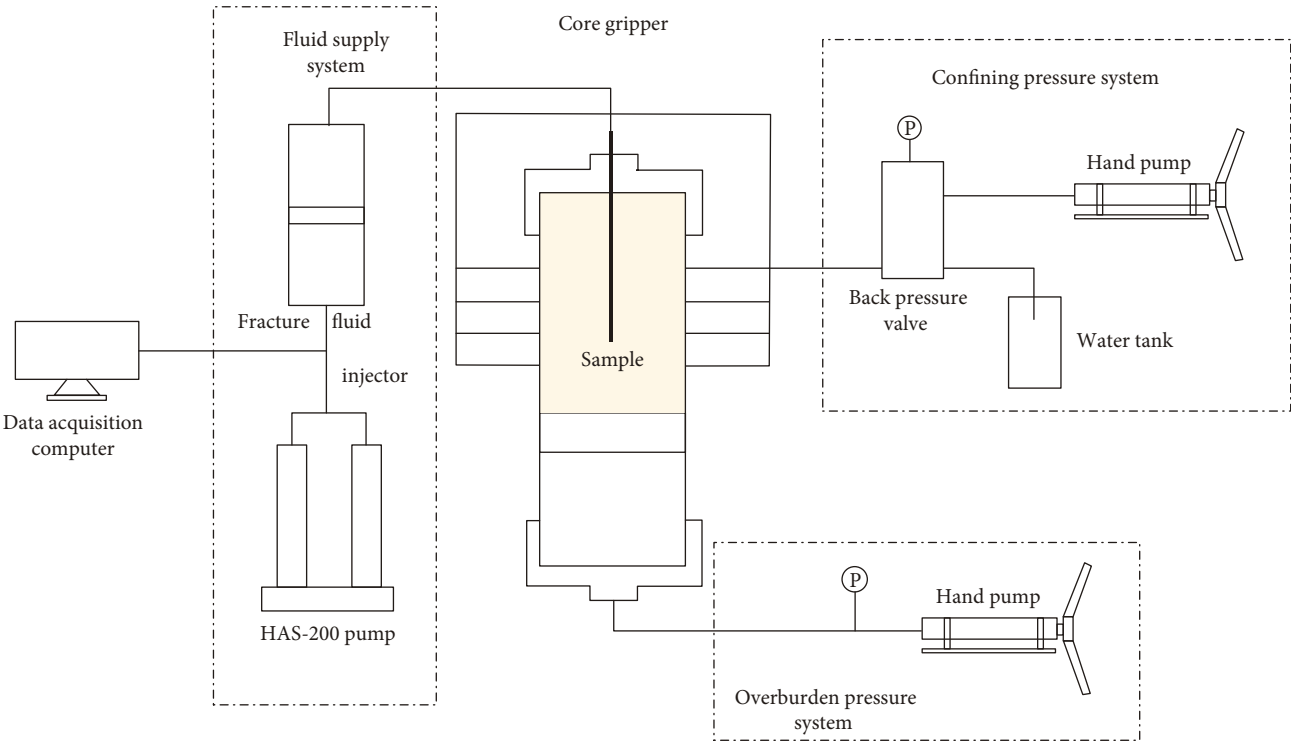

Figure 3: Schematic of hydraulic fracturing equipment.

Table 1: The details of hydraulic fracturing equipment parameters.

Parameters	Value
Volume of the core gripper	5 L
Maximum pressure resistance	32 MPa-40 MPa
Inner diameter of the fracturing pipe	4 mm
Outer diameter of the fracturing pipe	6 mm
Length of the fracturing pipe extending into the core gripper	18 cm

Figure 4: Clayey-silt sediments samples.

resistance to improve gas production. Previous studies that have verified brittleness index, mineral composition, hydrate saturation, fracturing fluid viscosity, and displacement are the main factors affecting the fracability of hydrate-bearing sediments [28–30]. Hydrate-bearing sandy sediments may form a cementing structure at higher saturations to possess consolidated rock-like mechanical properties due to the interconnected network of hydrates in pores or hydrates on sand grains [27, 31]. Thus, hydrate-bearing sandy sediments could be artificially fractured using hydraulic fracturing [32].

Up to now, majorities of research focus on the fracability of hydrate-bearing sandy sediments, but the studies rarely involved fracture propagation characteristics of clayey-silt sediments in the hydrate dissociation area. The formation energy depletes at the later stage of hydrate gas production, causing the decline in thermal and pressure conductivity of the reservoir, which is difficult to spread to the far end of the wellbore [33–35]. Meanwhile, lack of gas channel to flow

Table 2: Experimental design for fracturing on clayey-silt sediments.

Sample type	Confining pressure (MPa)	Overburden pressure (MPa)	Injection rate (ml/min)
1	10	10	10
2	10	10	10
3	15	10	10

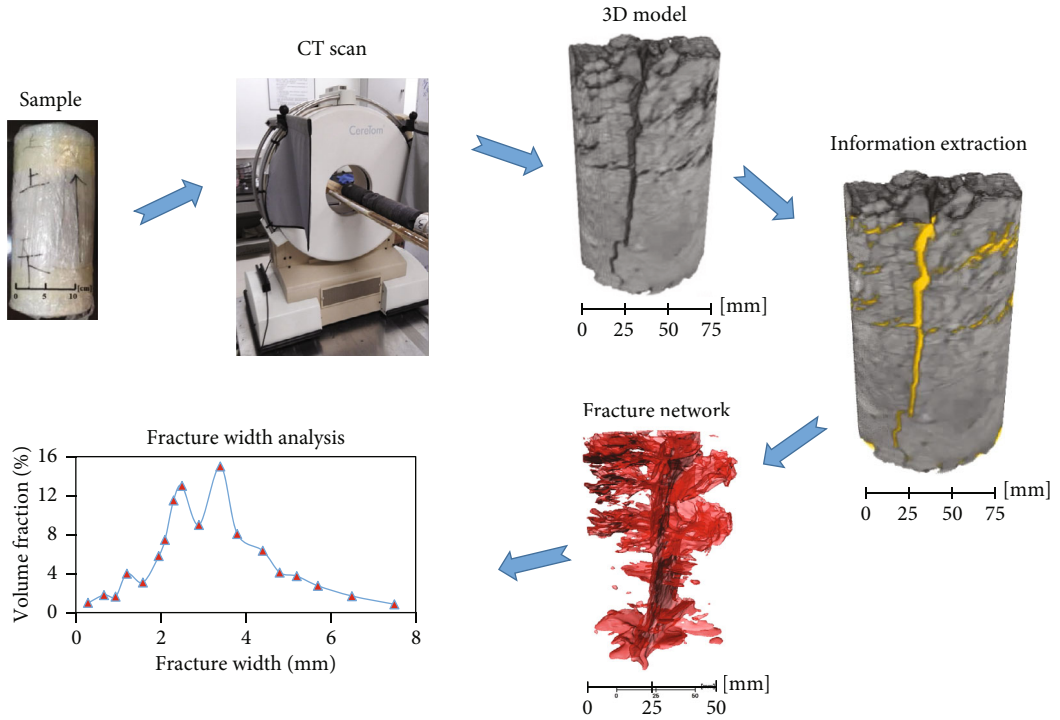

Figure 5: The process of CT scanning in clayey-silt sediments.

from the dissociation front to the wellbore, the gas production is seriously affected [36–39]. Therefore, the fracture propagation characteristics of clayey-silt sediments in hydrate dissociation are an important issue.

Ito et al. [40] used silica sand mixing kaolinite flour as laboratory synthesized samples to analyze hydraulic fracturing behavior in unconsolidated sands and indicated that fracturing fluid injection would create the fractures between the sand and the mud layers. Zhang et al. [41] experimentally investigated the influence of fracturing fluid viscosity on hydraulic fracturing and observed that high-viscosity fracturing fluid could induce higher breakdown pressure and complex fractures. Yang et al. [42] conducted a laboratory fracturing test in clay sediments to observe fracture propagation. They investigated that the vertical and horizontal fractures expanded synchronously and did not indicate significant directivity without confining pressure and overburden pressure. The high-pressure fluid penetrated the cavities in the clay sediments, forming areas of locally high pressure owing to the low permeability of clay sediments. As mentioned above, the laboratory fracturing test is an effective and direct method for analyzing fracture propagation mechanism. However, revealing the spatial distribution of fractures should combine with other methods.

This paper carried out hydraulic fracturing experiments to analyze the fracability of clayey-silt sediments in the hydrate dissociation area of the Shenhu Area under different confining pressure. The influence of the confining pressure on fracture initiation and propagation was discussed based on CT scanning. The results provide theoretical support for the research on hydraulic fracturing in clayey-silt sediments of the hydrate dissociation area.

2. Samples and Experiment Method

2.1. Samples. The tested samples composed of clayey-silt sediments with a median particle size of 12 μm are from the surface of the seabed in the Shenhu area. Clay and quartz are dominant, which account for 47.2% and 36.4%, respectively. The clay minerals are mainly montmorillonite and illite [19, 37].

The particles with a diameter of 0.005 mm-0.05 mm account for about 80%. Figure 2 shows the stress-strain relationship of clayey-silt sediments that belongs to plastic failure. When the strain reaches 2%, the undrained shear

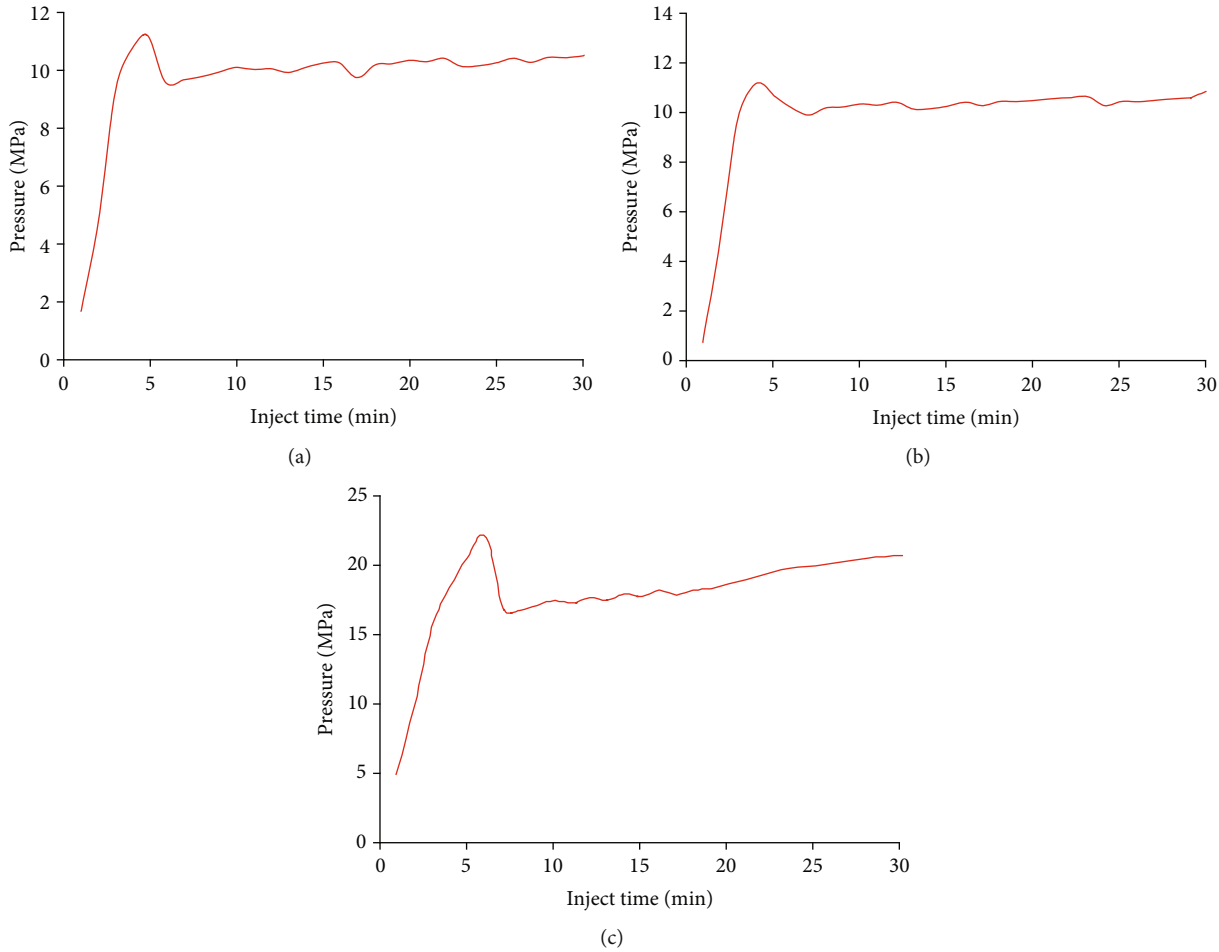

Figure 6: Changes in the injection pressure in samples 1 (a), 2 (b), and 3 (c) during hydraulic fracturing.

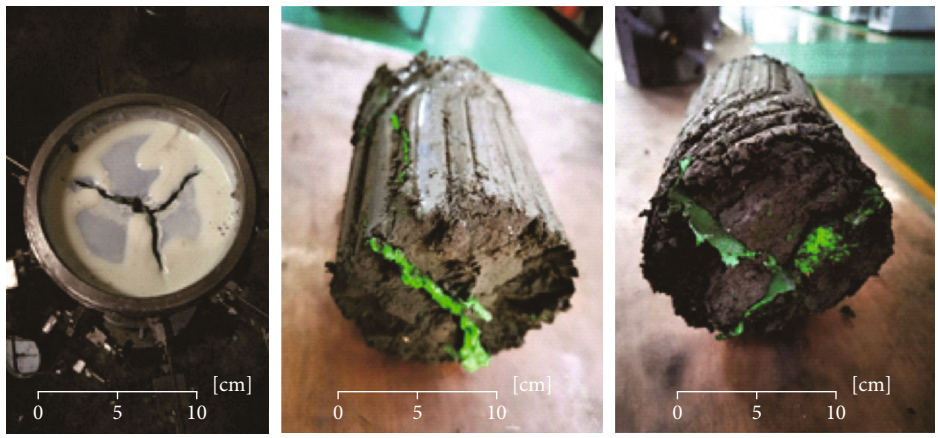

Figure 7: The fracture morphology in clayey-silt sediments.

strength reaches the peak value. When the strain exceeds 2%, the stress basically does not increase or slightly decreases. The effective cohesion and internal friction angle account for 0.04 MPa and 0.5°, respectively [43, 44].

2.2. Apparatus. A schematic of hydraulic fracturing equipment is shown in Figure 3. The equipment mainly consists of core gripper, fracturing pipe, fluid supply system, overburden pressure system, confining pressure system, and data acquisition system [45]. Table 1 presents the details of the equipment parameters. The fracturing fluid is injected via the HAS-200 pump. Uniform radial pressure and axial pressure are possessed to simulate in situ stresses.

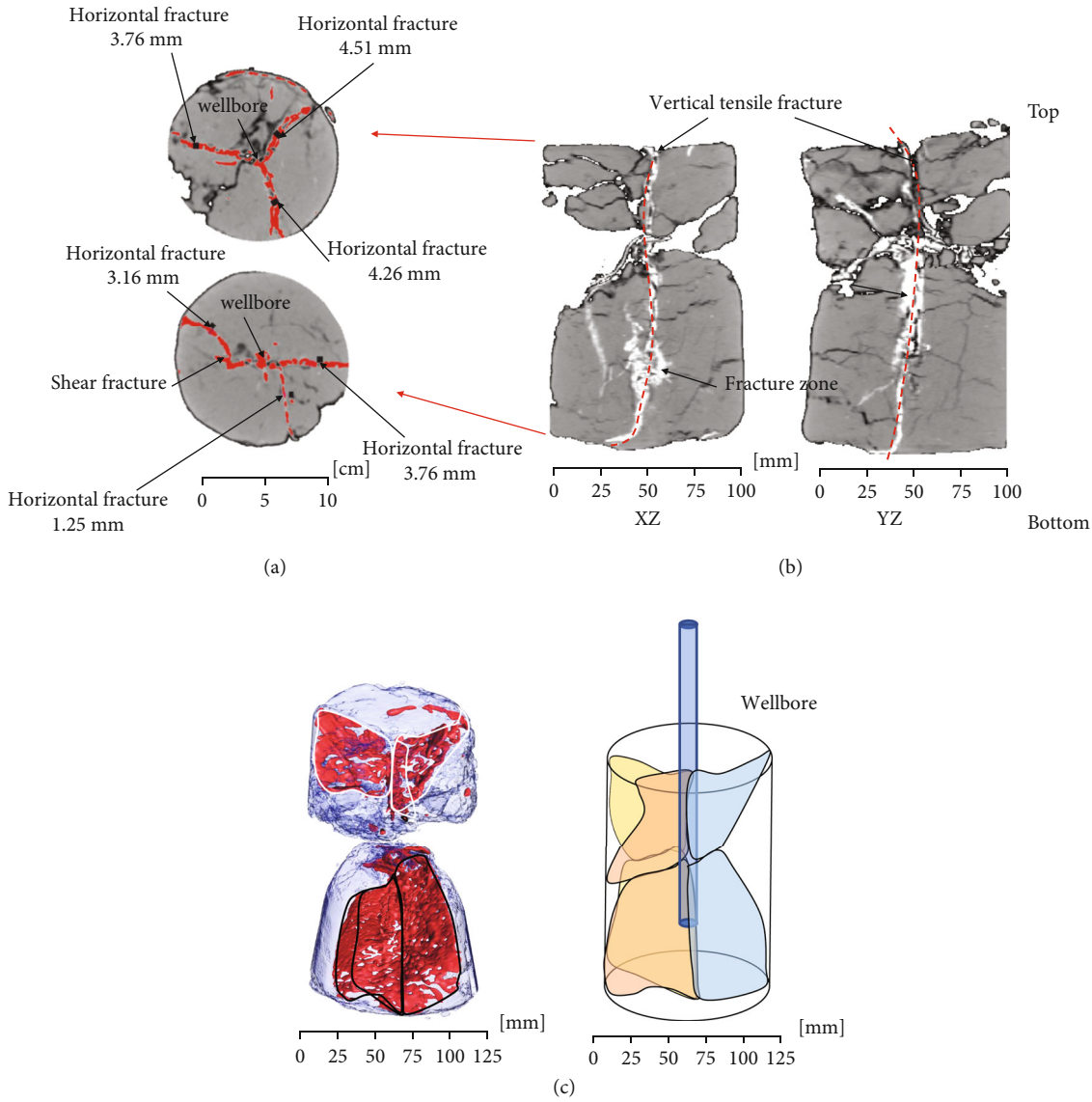

FIGURE 8: The fracture characteristics of sample 1 after hydraulic fracturing by CT: (a) CT section image, (b) CT perspective views, and (c) 3D illustration.

Fluorescent paint with a viscosity of 70 mPa·s was selected as fracturing fluid, which could be filled in fractures after drying to increase the discernibility of fractures. During the experiments, three sets of samples were designed. The samples sizes were 13 cm (diameter) × 27 cm (height), 13 cm (diameter) × 15 cm (height), and 13 cm (diameter) × 15 cm(height), respectively.

Dry clayey-silt sediments were compacted in the core gripper by the stick to produce the core sample with the porosity derived by the mass balance of 39% (Figure 4). To prevent pipelines from being blocked by the samples, the wire mesh and asbestos paper were placed on the inner wall of the core gripper. Then, the confining and overburden pressure was maintained constant as Table 2. The fracturing fluid was injected into the core gripper at a speed of 10 ml/min. After fracturing, the core gripper without the pipeline was put into the oven at a temperature of 50°C to help the fracturing fluid to fill in the fractures for convenient observation and avoid more fractures caused by sample dehydration. Meanwhile, low temperature drying is an effective method for taking out the sample to maintain the integrity of fractures. Finally, the samples were scanned by a CT scanner (Neuro-Logica Corporation, CereTom) to detect the fractures with a resolution of 0.5 mm × 0.5 mm × 0.625 mm and a single exposure time of 0.5 s. The three-dimensional gray-scale images were processed by collecting the X-ray attenuation information to obtain the segmentation image via Avizo software that could be utilized for fracture network modeling. Then, the fracture information was extracted based on the ball-stick model to reveal the spatial distribution of fractures, as shown in Figure 5 [39, 46]. Especially, note that the fractures with smaller widths should not be in the study since the sample heating will produce some fractures.

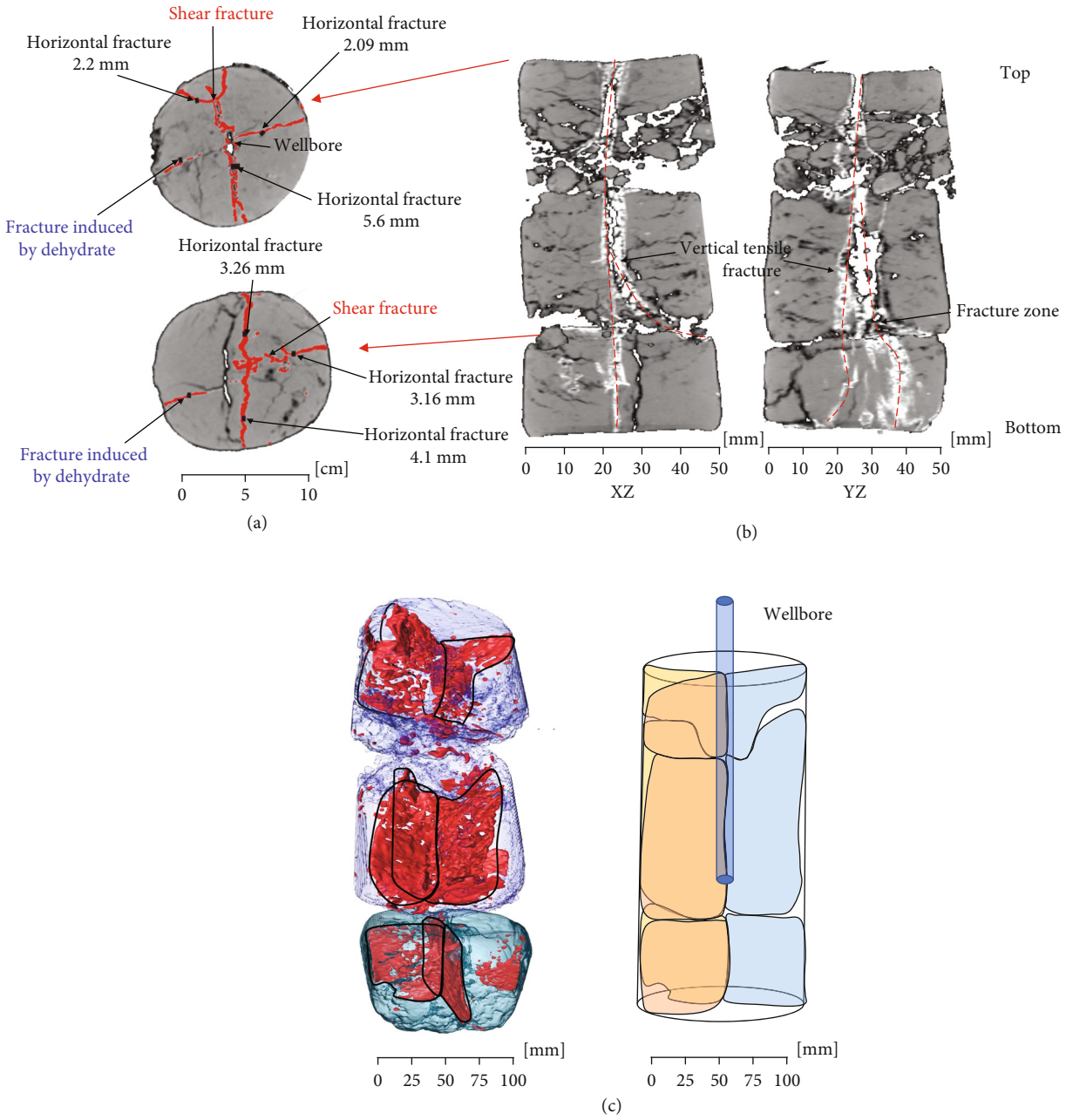

FIGURE 9: The fracture characteristics of sample 2 after hydraulic fracturing by CT: (a) CT section image, (b) CT perspective views, and (c) 3D illustration.

3. Results and Discussion

3.1. Fracturing Behavior with Confining Pressure of 10 MPa. The injection pressure curve reflects the fracturing behavior in clayey-silt sediments. Figures 6(a) and 6(b) show the injection pressure changes for two samples during hydraulic fracturing. The injection pressure rapidly increased for short injections to a peak and then drop to a plateau, which indicates that hydraulic fractures and microfractures were induced. The breakdown pressure of samples 1 and 2 was approximately 11.5 MPa and 11 MPa, respectively. Owing to the low permeability of the samples, the injection pressure fluctuated constantly in the process of hydraulic fracturing.

Several fractures were induced by hydraulic fracturing in clayey-silt sediments. A main fracture was in the center of the sample and propagated through the entire sample with a width of 6 mm. Some discontinuity fractures could be observed on the side of the sample, as shown in Figure 7.

The fracture morphology of the samples by CT scan was utilized to further analyze the fracture initiation and propagation mechanism of clayey-silt sediments. Three horizontal fractures were formed at the top of sample 1 with a length of 6.5 cm, and the width was 3.76 mm, 4.26 mm, and 4.51 mm, respectively, while the width of the fractures at the bottom of the sample was 6 mm, 6.5 mm, and 7.5 mm, respectively, as shown in Figure 8(a).

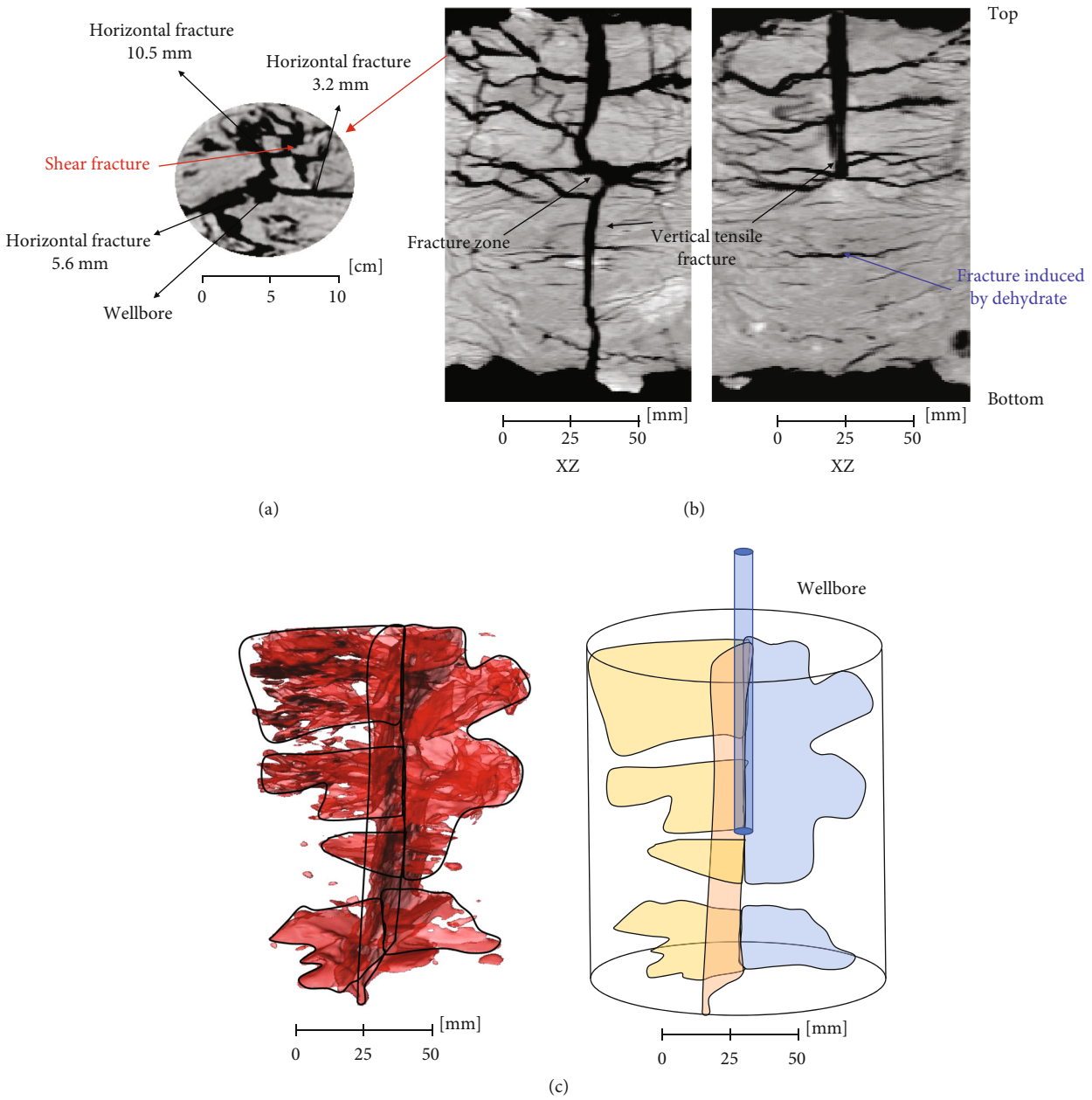

Figure 10: The fracture characteristics of sample 3 after hydraulic fracturing by CT: (a) CT section image, (b) CT perspective views, and (c) 3D illustration.

The vertical fracture of sample 1 propagated, connected, and communicated the branched fractures and microfractures induced by shear failure near the wellbore. Hence, the propagation and widening alternated to form a high-density fracture zone (Figure 8(b)). At the same time, several continuous horizontal fractures were observed around the wellbore, connected the microfractures, which showed an abnormal increase in the width of some fractures (Figure 8(a)). Due to the natural fractures by uneven sample filling, some new initial stresses might generate on the original propagation. If the induced stress exceeded the corresponding rock strength, a turning fracture might be formed (Figure 8(c)).

Three horizontal fractures were formed at the top of sample 2 with a length of 6.5 cm, and the width was 2.2 mm, 2.09 mm, and 5.6 mm, respectively, while the width of the fractures at the bottom of the sample was 3.26 mm, 3.16 mm, and 4.1 mm, respectively, as shown in Figure 9(a). Due to the high plasticity of the clayey-silt sediments, branching off often appeared in shear failure occurred. And the branched fractures propagated to the side of the sample (Figure 9(b)). At the same time, several horizontal fractures and fracture zones could be observed around the wellbore. However, lack of energy in the lower sample, microfractures were hard to connect and communicate with each other,

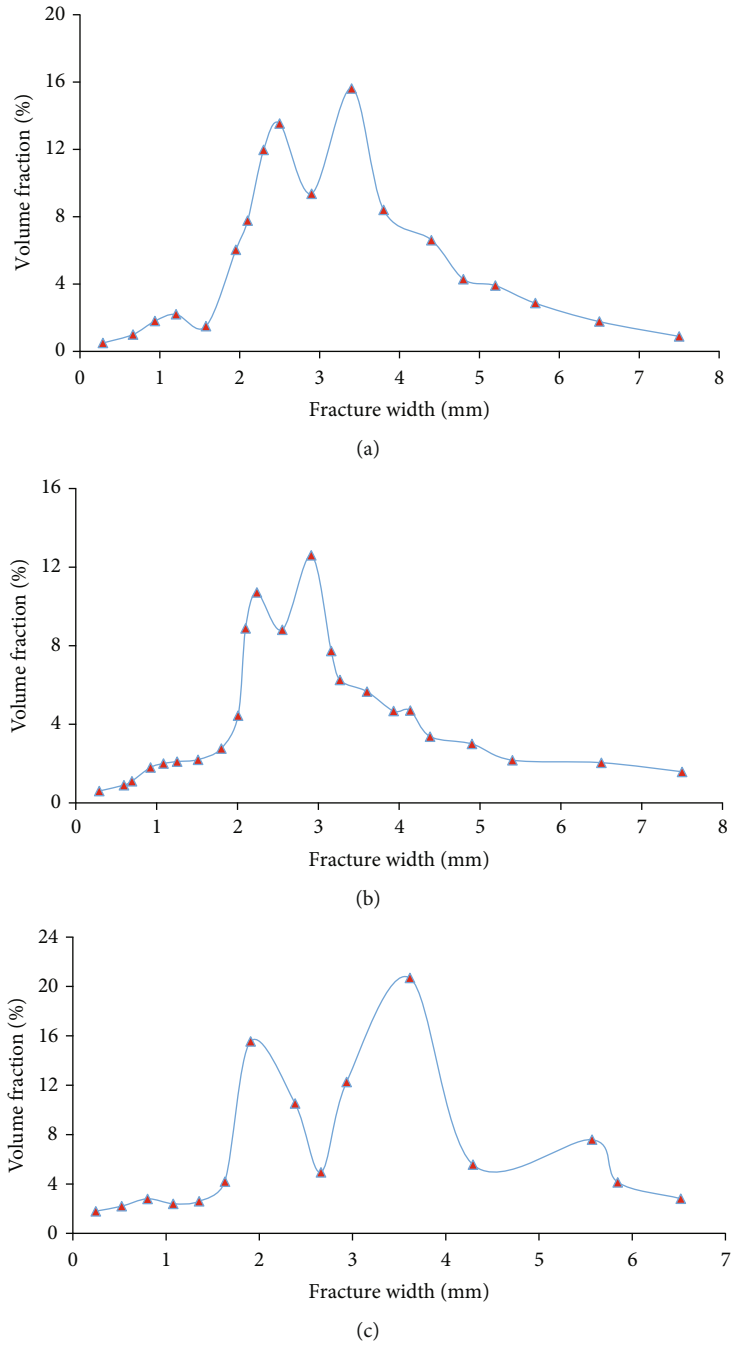

Figure 11: The fracture width of samples 1 (a), 2 (b), and 3 (c).

which could not merge with the main fracture to distribute in the sample independently (Figure 9(c)).

3.2. Fracturing Behavior with Confining Pressure of 15 MPa. Figure 6(c) demonstratesthat the injection pressure rapidly rose at the peak of 21.7 MPa, then decreased slightly and finally stabilized at approximately 20 MPa. Additionally, in contrast to cases with low confining pressure, the breakdown pressure of sample 3 is higher than that for samples 1 and 2, which indicated that sample 3 required more energy to exceed the compressive strength increasing with confining pressure.

Three horizontal fractures were formed at the top of sample 3 with a length of 6.5 cm, and the width was 10.5 mm, 3.2 mm, and 5.6 mm, respectively (Figure 10(a)). The vertical fracture of Sample 3 deflected at a certain angle near the wellbore (Figure 10(b)). Independent fracture could be observed around the wellbore. The horizontal fractures in the lower sample with short extended length were poorly developed, which could not penetrate the sample. Therefore, only two horizontal fractures could be observed at the bottom of sample 3 (Figure 10(c)).

Due to the high plasticity of clayey-silt sediments, fracturing fluid leakage was small, which produced an expansion

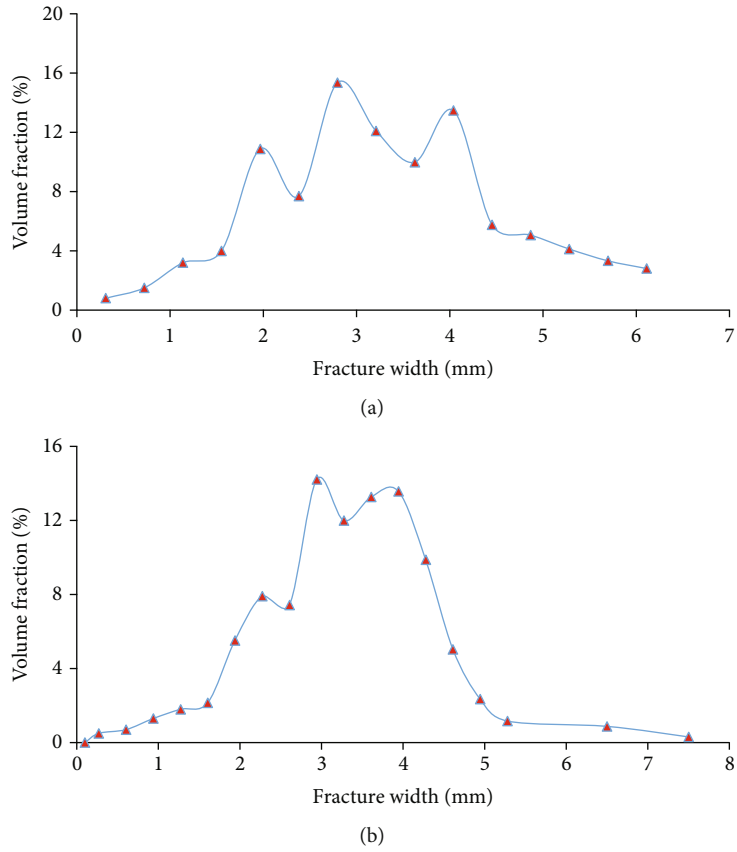

Figure 12: The fracture width of sample at the top (a) and bottom (b).

pressure. The shear failure occurred at the tip of the tensile fracture. After the shear expansion, the fracturing fluid continued to penetrate. The permeable zone often became shear a failure zone.

3.3. Discussions. Previous studies indicate that the complexity of fracture geometry has a great relationship with the rock brittleness in hydraulic fracturing [47–49]. As the brittleness increases, the hydraulic fracture geometry becomes more complex [50]. And as brittleness decreases, the fracture becomes more like biwing fracture geometry. Clayey-silt sediments are high in content of clay mineral swelled with water to greatly enhance the reservoir plasticity, resulting in more energy consumption in the formation to propagate and generate multiple fractures.

The mechanical characteristics of the reservoir have a significant influence on fracture pressure, fracture width, and tensile shear failure mechanism, while the pore pressure gradient is the dominant factor controlling the fracture half-length and the influence degree of shear failure [31, 41]. Due to the low permeability of clayey-silt sediments, the injected fracture fluid easily maintains the high pressure near the wellbore. When the injection pressure is greater than the breakdown pressure, the samples begin to generate fractures. Additionally, clayey-silt sediments near the wellbore are prone to plastic yield, and the stress concentration is weakened, which are affected by plasticity and fluid leak-off. Therefore, tensile and shear failure occurs simultaneously during fracture initiation. By the invasion of fracture fluid and the increase of pore pressure, shear failure occurs at the fracture tip, and then the fracture tip fails subjected to tensile stress, resulting in the propagation of clayey-silt sediments.

The initial stress of fracture propagation is generated different from that of the original path affected by the heterogeneity and the existence of internal weak structural plane, At the same time, the friction between fracturing fluid and clayey-silt particles also causes lots of subtle shear failure in the fracture propagation process, resulting in the fracture instability to form turning fractures or even multibranched fractures, and microfractures, and fracture zones can be observed around the main fracture. And the fracture surface becomes rougher with a small number of sediment particles peeling off.

To obtain the fracture information accurately, the width of the samples was analyzed by using the ball-stick model, as shown in Figure 11. When the confining pressure was 10 MPa, the fracture width ranged from 0 mm to 7.5 mm, and three peaks were 1.2 mm, 2.5 mm, and 3.4 mm, respectively. The fractures with a width of 1.2 mm-3.4 mm accounted for 68% of the fracture volume (Figures 11(a) and 11(b)). When the confining pressure was 15 MPa, the fracture width ranged from 0 mm to 6.5 mm, and the peaks of the curve obviously shifted to the right, which were 1.9 mm, 3.6 mm, and 5.6 mm, respectively. The fractures with a width of 1.9 mm-5.6 mm accounted for 77% of the fracture volume (Figure 11(c)). The increasing width indicated that

the hydraulic fracturing effect of fracturing fluid on fractures was enhanced continuously with the confining pressure.

0 mm-2 mm fractures with high confining pressure accounted for 31% of the total volume, while 0 mm-2 mm fractures with low confining pressure only accounted for 13% of the total volume, which indicated that the plasticity of clayey-silt sediments with high confining pressure was stronger, and plastic expansion occurred easily. In the hydraulic fracturing process, the sediments near the wellbore were continuously squeezed, and plastic deformation occurs to generate numerous microfractures.

Under the same confining pressure, the fractures at the top were generally wider than those at the bottom, and the width was mainly 1.2 mm-6 mm (Figure 12(a)). In contrast, the width of the fracture at the bottom was mainly 1 mm-5 mm. Additionally, the curve crest obviously shifted to the left (Figure 12(b)), which might be the result of lack of energy in the lower sample. Microfractures were hard to connect and communicate with each other to form wider fractures.

4. Conclusion

The hydraulic fracturing experiments were conducted to analyze the fracability of clayey-silt sediments in the hydrate dissociation area of the Shenhu Area under different confining pressure. The fracture behavior as a consolidated rock-like fracturing mode was observed. Owing to the high content of clay mineral swelled with water to greatly enhance the reservoir plasticity, formation requires more energy consumption to propagate and generate tensile fractures and local shear fractures. The plasticity of clayey-silt sediments with high confining pressure is stronger, and plastic expansion occurs easily. When the confining pressure was 15 MPa, the fractures were mainly composed of 1.9 mm-5.6 mm wide fractures, accounting for 77% of the total volume. When the confining pressure was 10 MPa, the fractures were mainly composed of 1.5 mm-3.4 mm wide fractures, accounting for 68% of the total volume. The fracture width increases with the confining pressure.

The influence of the confining pressure on fracture initiation and propagation based on CT scanning in this paper could serve as a reference in the research on hydraulic fracturing in clayey-silt sediments of the hydrate dissociation area. It is noted that the effect of low temperature and fracture fluid is not taken into account in this paper. Thus, some of the future considerations relating to the fracability of clayey-silt sediments may include examining the (1) effects of low temperature to simulate closely to the real application (2) effects of fracture fluid and proppant and (3) larger studies to observe more fracture propagation behaviors.

Data Availability

The data used to support the findings of this study are available from the corresponding author upon request.

Conflicts of Interest

The authors declare that they have no conflicts of interest.

Acknowledgments

The authors are grateful to the National Natural Science Foundation of China (51991365), Key Special Project for Introduced Talents Team of Southern Marine Science and Engineering Guangdong Laboratory (Guangzhou) (GML2019ZD0105), Key Program of Marine Economy Development (Six Marine Industries) Special Foundation of Department of Natural Resources of Guangdong Province [2020]047, and China Geological Survey Project (DD20211350).

References

[1] Y. F. Makogon, S. A. Holditch, and T. Y. Makogon, "Natural gas-hydrates – a potential energy source for the 21st Century," *Journal of Petroleum Science and Engineering*, vol. 56, no. 1-3, pp. 14–31, 2007.

[2] B. Anderson, S. Hancock, S. Wilson et al., "Formation pressure testing at the mount Elbert gas hydrate stratigraphic test well, Alaska North Slope: operational summary, history matching, and interpretations," *Marine and Petroleum Geology*, vol. 28, no. 2, pp. 478–492, 2011.

[3] K. Egawa, O. Nishimura, S. Izumi et al., "Bulk sediment mineralogy of gas hydrate reservoir at the East Nankai offshore production test site," *Marine and Petroleum Geology*, vol. 66, pp. 379–387, 2015.

[4] Z. R. Wu, Y. H. Li, X. Sun, P. Wu, and J. Zheng, "Experimental study on the effect of methane hydrate decomposition on gas phase permeability of clayey sediments," *Applied Energy*, vol. 230, pp. 1304–1310, 2018.

[5] R. Boswell and T. S. Collett, "Current perspectives on gas hydrate resources," *Energy and Environmental Science*, vol. 4, no. 4, pp. 1206–1215, 2011.

[6] S. Dai, J. Kim, Y. Xu et al., "Permeability anisotropy and relative permeability in sediments from the National gas Hydrate Program Expedition 02, offshore India," *Marine and Petroleum Geology*, vol. 108, pp. 705–713, 2019.

[7] Y. Konno, J. Yoneda, K. Egawa et al., "Permeability of sediment cores from methane hydrate deposit in the eastern Nankai Trough," *Marine and Petroleum Geology*, vol. 66, pp. 487–495, 2015.

[8] E. D. Sloan, "Fundamental principles and applications of natural gas hydrates," *Nature*, vol. 426, no. 6964, pp. 353–359, 2003.

[9] F. Colwell, R. Matsumoto, and D. Reed, "A review of the gas hydrates, geology, and biology of the Nankai trough," *Chemical Geology*, vol. 205, no. 3-4, pp. 391–404, 2004.

[10] N. Mahabadi, S. Dai, Y. Seol, T. Sup Yun, and J. Jang, "The water retention curve and relative permeability for gas production from hydrate-bearing sediments: pore-network model simulation," *Geochemistry, Geophysics, Geosystems*, vol. 17, no. 8, pp. 3099–3110, 2016.

[11] S. Dai and Y. Seol, "Water permeability in hydrate-bearing sediments: a pore-scale study," *Geophysical Research Letters*, vol. 41, no. 12, pp. 4176–4184, 2014.

[12] J. Yoneda, M. Oshima, M. Kida et al., "Permeability variation and anisotropy of gas hydrate-bearing pressure-core sediments recovered from the Krishna-Godavari Basin, offshore India," *Marine and Petroleum Geology*, vol. 108, pp. 524–536, 2019.

[13] H. Singh, N. Mahabadi, E. M. Myshakin, and Y. Seol, "A mechanistic model for relative permeability of gas and water flow in hydrate-bearing porous media with capillarity," *Water Resources Research*, vol. 55, no. 4, pp. 3414–3432, 2019.

[14] M. Ghiasi, A. Bahadori, S. Zendehboudi, A. Jamili, and S. Rezaei-Gomari, "Novel methods predict equilibrium vapor methanol content during gas hydrate inhibition," *Journal of Natural Gas Science and Engineering*, vol. 15, pp. 69–75, 2013.

[15] L. Chen, Y. C. Feng, T. Kogawa, J. Okajima, A. Komiya, and S. Maruyama, "Construction and simulation of reservoir scale layered model for production and utilization of methane hydrate: the case of Nankai trough Japan," *Energy*, vol. 143, pp. 128–140, 2018.

[16] S. Sakurai, I. Nishioka, M. Matsuzawa, B. Matzain, A. Goto, and J. E. Lee, "Issues and challenges with controlling large drawdown in the first offshore methane hydrate production test," in *SPE Asia Pacific Oil & Gas Conference and Exhibition*, Perth, Australia, 2016.

[17] L. Chen, Y. Feng, J. Okajima, A. Komiya, and S. Maruyama, "Production behavior and numerical analysis for 2017 methane hydrate extraction test of Shenhu, South China Sea," *Journal of Natural Gas Science and Engineering*, vol. 53, pp. 55–66, 2018.

[18] J. F. Li, J. L. Ye, X. W. Qin et al., "The first offshore natural gas hydrate production test in South China Sea," *China Geology*, vol. 1, no. 1, pp. 5–16, 2018.

[19] J. L. Ye, X. W. Qin, W. W. Xie et al., "The second natural gas hydrate production test in the South China Sea," *China Geology*, vol. 2, pp. 197–209, 2020.

[20] T. Yu, G. Guan, A. Abudula, A. Yoshida, D. Wang, and Y. Song, "Gas recovery enhancement from methane hydrate reservoir in the Nankai Trough using vertical wells," *Energy*, vol. 166, pp. 834–844, 2019.

[21] C. Chen, L. Yang, R. Jia et al., "Simulation study on the effect of fracturing technology on the production efficiency of natural gas hydrate," *Energies*, vol. 10, no. 8, p. 1241, 2017.

[22] L. Yang, C. Chen, R. Jia et al., "Influence of reservoir stimulation on marine gas hydrate conversion efficiency in different accumulation conditions," *Energies*, vol. 11, no. 2, p. 339, 2018.

[23] Z. Y. Wang, Y. Q. Liao, W. D. Zhang, B. Sun, X. Sun, and X. Deng, "Coupled temperature field model of gas-hydrate formation for thermal fluid fracturing," *Applied Thermal Engineering*, vol. 133, pp. 160–169, 2018.

[24] Y. C. Feng, L. Chen, A. Suzuki et al., "Enhancement of gas production from methane hydrate reservoirs by the combination of hydraulic fracturing and depressurization method," *Energy Conversion and Management*, vol. 184, pp. 194–204, 2019.

[25] J. X. Sun, F. L. Ning, T. L. Liu et al., "Gas production from a silty hydrate reservoir in the South China Sea using hydraulic fracturing: a numerical simulation," *Energy Science & Engineering*, vol. 7, no. 4, pp. 1106–1122, 2019.

[26] M. Enderlin, H. Alsleben, and J. Beyer, "Predicting fracability in shale reservoirs," in *AAPG Annual Convention and Exhibition*, pp. 10–13, Houston, Texas, USA, 2011.

[27] J. L. Too, A. Cheng, and A. P. Linga, "Fracturing methane hydrate in sand: a review of the current status," in *Offshore Technology Conference Asia*, Kuala Lumpur, Malaysia, 2018.

[28] Y. Konno, Y. Jin, J. Yoneda, T. Uchiumi, K. Shinjou, and J. Nagao, "Hydraulic fracturing in methane-hydrate-bearing sand," *RSC Advances*, vol. 6, no. 77, pp. 73148–73155, 2016.

[29] J. L. Too, A. Cheng, B. C. Khoo, A. Palmer, and P. Linga, "Hydraulic fracturing in a penny-shaped crack. Part II: testing the frackability of methane hydrate-bearing sand," *Journal of Natural Gas Science and Engineering*, vol. 52, pp. 619–628, 2018.

[30] Y. C. Liu, M. G. Sun, G. T. Wang, Q. Wang, and L. Zhao, "An investigation of hydraulic fracturing applied to marine gas hydrate reservoirs," *Materials Science and Engineering*, vol. 729, article 012050, 2020.

[31] X. Q. Liu, W. D. Zhang, Z. Q. Qu et al., "Feasibility evaluation of hydraulic fracturing in hydrate-bearing sediments based on analytic hierarchy process-entropy method (AHP-EM)," *Journal of Natural Gas Science and Engineering*, vol. 81, article 103434, 2020.

[32] J. W. Jung and J. C. Santamarina, "Hydrate adhesive and tensile strengths," *Geochemistry, Geophysics, Geosystems*, vol. 12, no. 8, 2011.

[33] G. J. Moridis, T. S. Collett, M. Poolad-Darvish et al., *Challenges, uncertainties and issues facing gas production from gas hydrate deposits*, Lawrence Berkeley National Laboratory, Berkeley, CA, 2010.

[34] X. Ge, J. Liu, Y. Fan, D. Xing, S. Deng, and J. Cai, "Laboratory investigation into the formation and dissociation process of gas hydrate by low-field NMR technique," *Journal of Geophysical Research Solid Earth*, vol. 123, no. 5, pp. 3339–3346, 2018.

[35] L. Yang, C. Zhang, J. Cai, and H. Lu, "Experimental investigation of spontaneous imbibition of water into hydrate sediments using nuclear magnetic resonance method," *Energies*, vol. 13, no. 2, p. 445, 2020.

[36] X. Liu, C. Liu, J. Wu et al., "Dynamic characteristics of offshore natural gas hydrate dissociation by depressurization in marine sediments," *Geofluids*, vol. 2019, Article ID 6074892, 11 pages, 2019.

[37] C. Lu, Y. Xia, X. Sun et al., "Permeability evolution at various pressure gradients in natural gas hydrate reservoir at the Shenhu area in the South China Sea," *Energies*, vol. 12, no. 19, 2019.

[38] S. Wang, D. Luo, X. Zhang, X. Lu, and Y. Shi, "Experimental study on mechanical properties of hydrated clay," *Journal of Experiment Mechanics*, vol. 33, no. 2, pp. 245–252, 2018.

[39] J. Cai, Y. Xia, C. Lu, H. Bian, and S. Zou, "Creeping microstructure and fractal permeability model of natural gas hydrate reservoir," *Marine and Petroleum Geology*, vol. 115, p. 104282, 2020.

[40] T. Ito, A. Igarashi, K. Suzuki et al., "Laboratory study of hydraulic fracturing behavior in unconsolidated sands for methane hydrate production," in *Offshore Technology Conference*, Houston, Texas, USA, 2008.

[41] W. D. Zhang, X. Shi, S. Jiang et al., "Experimental study of hydraulic fracture initiation and propagation in highly saturated methane-hydrate-bearing sands," *Journal of Natural Gas Science and Engineering*, vol. 79, article 103338, 2020.

[42] L. Yang, F. K. Shi, and J. Yang, "Experimental studies on hydraulic fracturing in hydrate sediment," *Chemistry and Technology of Fuels and Oils*, vol. 56, no. 1, pp. 107–114, 2020.

[43] X. H. Zhang, X. B. Lu, L. M. Zhang, S. Y. Wang, and Q. P. Li, "Experimental study on mechanical properties of methane-hydrate-bearing sediments," *Acta Mechanica Sinica*, vol. 28, no. 5, pp. 1356–1366, 2012.

[44] X. B. Lu, X. H. Zhang, and S. Y. Wang, "Advances in study of mechanical properties of gas hydrate bearing sediments," *The Open Ocean Engineering Journal*, vol. 6, no. 1, pp. 26–40, 2013.

[45] X. Qin, J. Ye, H. Qiu et al., "An fracturing experimental equipment for clayey-silt reservoir," *Patent CN208605173U*, 2019.

[46] N. Watanabe, N. Hirano, N. Tsuchiya et al., "Three dimensional numerical analysis of fluid flow through fractured rock core using X-ray computed tomography," in *IPTC 2009: International Petroleum Technology Conference*, Doha, Qatar, 2009.

[47] R. Rickman, M. J. Mullen, J. E. Petre et al., "A practical use of shale petrophysics for stimulation design optimization: all shale plays are not clones of the Barnett shale," in *SPE Annual Technical Conference and Exhibition*, pp. 1–11, Denver, Colorado, USA, 2008.

[48] M. Mullen and M. Enderlin, "Fracability index-more than just calculating rock properties," in *SPE Annual Technical Conference and Exhibition*, San Antonio, Texas, USA, 2012.

[49] Z. Li, L. Li, M. Li et al., "A numerical investigation on the effects of rock brittleness on the hydraulic fractures in the shale reservoir," *Journal of Natural Gas Science and Engineering*, vol. 50, pp. 22–32, 2018.

[50] M. Kasim and A. Shakoor, "An investigation of the relationship between uniaxial compressive strength and degradation for selected rock types," *Lithos*, vol. 177, pp. 54–60, 2013.